EUROPEAN FUSION DEVELOPMENT AGREEMENT

EFDA–JET–PR(00)08

Reconstruction of the Power Deposition Profiles using JET MkIIGB Thermocouple Data for ELMy H-mode Plasmas

V Riccardo et al

EFDA–JET–PR(00)08

Reconstruction of the Power Deposition Profiles using JET MkIIGB Thermocouple Data for ELMy H-mode Plasmas

V Riccardo, G F Matthews, W Fundamenski.

EURATOM/UKAEA Fusion Association, Culham Science Centre, Abingdon, Oxfordshire, OX14 3DB, UK.

Preprint of a Paper to be submitted for publication in
Plasma Physics and Controlled Fusion

December 2000

ABSTRACT

Thermocouples (>40) are located ~10 mm below the surface in the tiles of the MkIIGB JET divertor. The time response of the temperature can be used to reconstruct the power deposition profile, when the strike point is slowly (up to 20 mm/s) moved along the tile.

This novel technique relies on finite element simulations to obtain the profile shape which best fits the measured temperature history at the thermocouple. The spatial accuracy of the profile along the strike point path is limited to a length similar to the distance of the thermocouple from the surface: features smaller that 10 mm can hardly be resolved.

Experiments with neutral beam heating power varying between 4 and 16 MW have been modelled both on the outer and on the inner strike point. It has been found that a single exponential description of the power profile is unable to fully fit the time derivative of the temperature at the outer strike point for H-mode discharges: an additional localised peak has to be added at the tip of the single exponential. This feature is present independently of the shift velocity and its magnitude decreases when the amount of gas puffed in the divertor region is increased. Scaling laws for the peak power density and the power decay length have been derived for a limited set of discharges.

1. INTRODUCTION

The characterisation of the scrape-off-layer parameters is determinant to the divertor design of next step devices, like ITER-FEAT [1] and FIRE [2], as well as for the heating upgrade of JET [3]. The peak power density, determined by the width of the scrape-off-layer, together with the material power loading capabilities and physical erosion yields, set a constrain on the divertor design and the plasma core performance.

Reliable measurements of the power deposition profile are necessary for the study of the power flux peak and width scalings that provide the design criteria for future machines. The deposition profiles are traditionally measured either by Langmuir probes [4] or by infrared cameras [5]. Power profiles derived from Langmuir probes are uncertain because the sheath power transmission factor depends also on the ion temperature, which is not measured. Infra-red diagnostics can provide a more direct measure of power deposition but can suffer from uncertainties on the surface emissivity, from the presence of surface layers with poor thermal contact and from infra-red emission from the plasma itself. A novel technique, based on divertor thermocouples and relying on finite element simulations, has been developed at JET and it will be described in this paper. It provides a reliable measure of the average power profile as experienced by the bulk material and is complementary to the other techniques.

Finite Element (FE) analysis had already been applied to a set of discharges run at constant plasma and heating configuration with the strike-point located at different heights on the vertical

target of the JET MkIIGB [6]. The power deposition profile obtained in this way is very reliable, but also very expensive in terms of the number of discharges needed at any given set of plasma conditions. However, the thermocouple time response is fast enough to be used to reconstruct the power deposition profile from a single discharge, if the strike-point is shifted across the thermocouple location slowly enough (some tens of mm/s). With a limited number of discharges, outer and inner power profile have been obtained for a range of input heating powers (4 to 16 MW) and D-puffing rates (0-3 10^{22} s^{-1}), both at the outer strike-point and, with a smaller confidence, at the inner strike-point.

The paper is organised as follow: in section 2 the FE model is described; in section 3 the accuracy of the method is discussed; in section 4 the method is validated; in section 5 the data collected in the JET-C1 campaign is summarised.

2. EXPERIMENTAL SET UP AND DESCRIPTION OF THE MODELS

Two of the 24 JET MkIIGB divertor modules have 21 thermocouples fitted within the Carbon Fibre Composite (CFC) target tiles at the locations shown in Figure 1. All the target tiles are in Dunlop 712 (a 2D CFC), apart from the ribs, which are in SEP-N11 (a quasi-3D CFC). Each module has two poloidal inner and outer baffle tiles, two poloidal inner and outer horizontal tiles, two poloidal dome tiles, but only one toroidal inner and outer vertical tiles. To optimise the mechanical performance of the tiles (avoid inter-weave cracks), the second good thermal conductivity direction in the vertical tiles is toroidal, while in the other tiles it is poloidal.

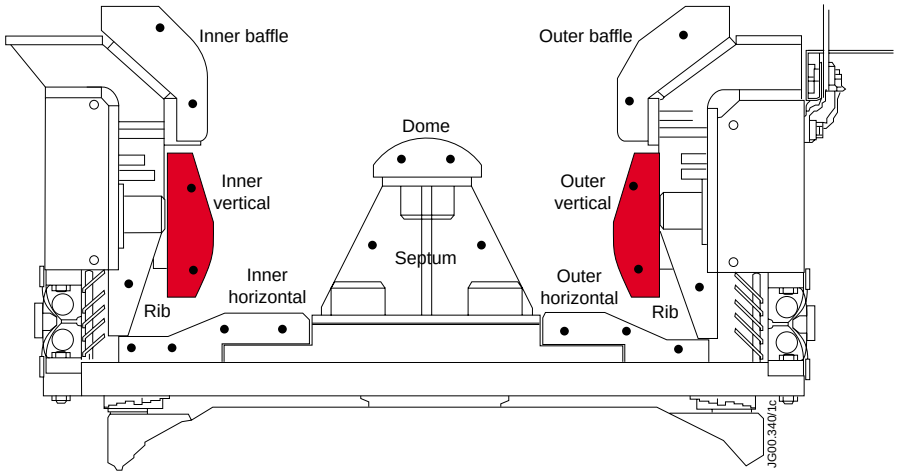

Figure 1: Poloidal section of the JET MkIIGB divertor target (thermocouples are marked by •)

The thermal properties of the 2D CFC had been measured on samples taken from the MkIIa and MkIIGB batches [7]. The average tile density is 1820 kg/m^3; the thermal properties, in particular the thermal conductivity which depends on the density, have been taken at this density. The parallel (along the two weave directions) and perpendicular thermal conductivity and the specific heat used in the simulations are plotted in Figure 2.

With the present divertor geometry, the pair of tiles where a shift of the plasma is easiest to perform is the vertical target. This has the additional advantage of having the CFC weave oriented toroidally: the poloidal conduction is minimised and therefore most of the power landing on the tile surface above the thermocouple is conducted directly to the thermocouple. Therefore, for this analysis, only the inner and outer vertical tiles have been modelled. The model of the outer tile is reported in Figure 3; where the precise location of its two thermocouples is indicated and also the boundary and loading conditions are summarised. The free faces of the tile have a radiation sink to the rest of the wall, the temperature of which does not change significantly during the power pulse away from the strike point region. Consequently the radiation sink temperature has been set to 200^0C (slightly higher than the usual tile initial temperature, which varies between 170^0C and 190^0C). The back face of the tile is discontinuously in contact with the carrier plate, to which the tile is attached through a dumbbell fixation. This complex and scattered heat sink has been replaced by fictitious convection at the back of the tile, the heat transfer coefficient of which has been set to match the long term cooling of the tile.

During the slow strike-point shift experiments (Figure 4), the vertical velocity of the strike-point is almost constant. The same plasma configuration has been run with neutral beam heating in the range of 4 to 16 MW at three vertical strike-point velocities: ~17 mm/s, ~9 mm/s and zero. When the velocity was larger than zero the starting

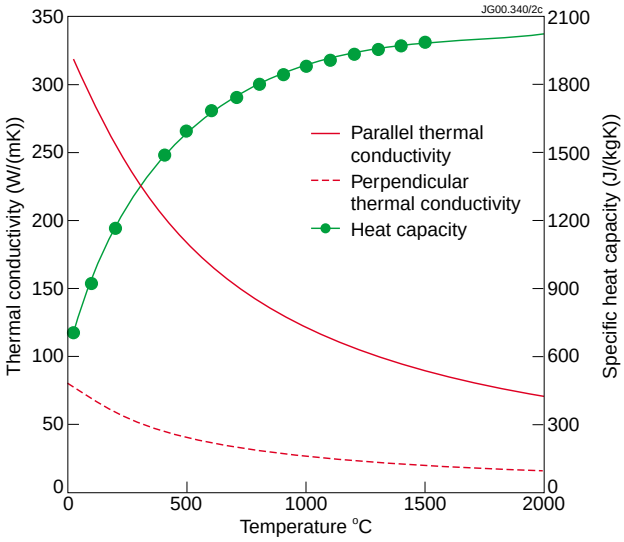

Figure 2: As-built thermal properties of the MKIIGB divertor tiles (parallel and perpendicular refer to the weave planes)

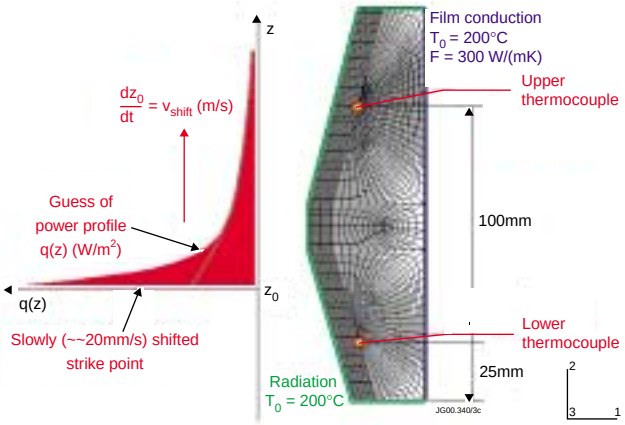

Figure 3: 2D model of the outer vertical tile. The two thermocouples are located 25 mm and 125 mm above the bottom end of the tile and ~10 mm behind the plasma facing surface. The top and bottom faces and the plasma facing surface radiate to a distant heat sink, whose temperature is assumed to be 200^0C. The film boundary condition at the back face of the tile represents the conduction through the dumbbell fixation and also the uneven thermal conduction and radiation to the carrier plate. The heat flux profile (perpendicular to the z-axis), used in the simulation is shown qualitatively.

position of the shift was set such that the top thermocouple in the lower vertical tiles was reached by the strike-point towards the end of its run; in the steady discharges instead the strike-point was kept just below the top

thermocouple. The uncertainty in the vertical position of the strike-point, as processed by EFIT, is taken into account by letting the initial position of the shift free to change within the error range (~20 mm), while the vertical velocity is kept constant.

For simplicity it has been assumed that the power profile shape does not change along the mean vertical line passing through the exposed tile surfaces while the plasma is moved upwards. This introduces an error, which will be discussed in the next section.

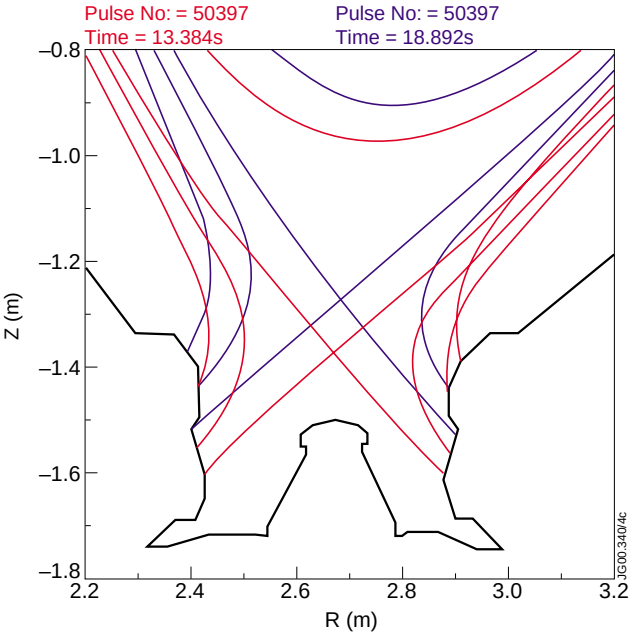

Figure 4: Pulse 50397 moved 100 mm upwards in 6 s

The power profile is described as the sum of two exponentials; originally a single exponential was used, but it could not match the full history of the measured time derivative. The thin exponential, l_T, controls the peak while the wide exponential, l_W, determines the tail of the time derivative of the temperature. The power density perpendicular to the z-axis can be broken into the wide (q_W) and thin (q_T) components,

$$q(z) = q_W(z) + q_T(z) = \frac{P_{leg}/\lambda_W}{1 - e^{-\frac{L}{\lambda_W}}} \frac{C\, e^{-\frac{z - z_{s-p}}{\lambda_W}}}{2\pi R (1 + C)} + \frac{P_{leg}/\lambda_T}{1 - e^{-\frac{L}{\lambda_T}}} \frac{e^{-\frac{z - z_{s-p}}{\lambda_T}}}{2\pi R (1 + C)},$$

with $C = P_W / P_T$, where $P_W = 2\pi R \int_0^L q_W(z)dz$ and $P_T = 2\pi R \int_0^L q_T(z)dz$.

The profile (projected on the effective length of the wetted element side) is given on segments 5 mm long (half the length which can be resolved with the thermocouples) and is moved in steps of 1 mm. The heat transfer calculation is divided in three steps. The first step models the heating and is done using a time increment which corresponds to a movement of 1 mm of the power profile. The second step covers the fast cooling which follows the end of the heating impulse (25 time increments of 1 s). The third step corresponds to the slow cooling (33 time increments of 30 s). The temperature is collected at the thermocouples after each time increment. The surface temperature and other energy parameters are saved at the end of each step.

The power profile for each discharge has been determined by matching the measured thermocouple temperature (Figure 5a), and its time derivative (Figure 5b), with those computed with the 2D model of the tile. A parameter, which has always been kept constant at the measured value, is the vertical velocity of the strike-point. Knowing the velocity and the time of the peak

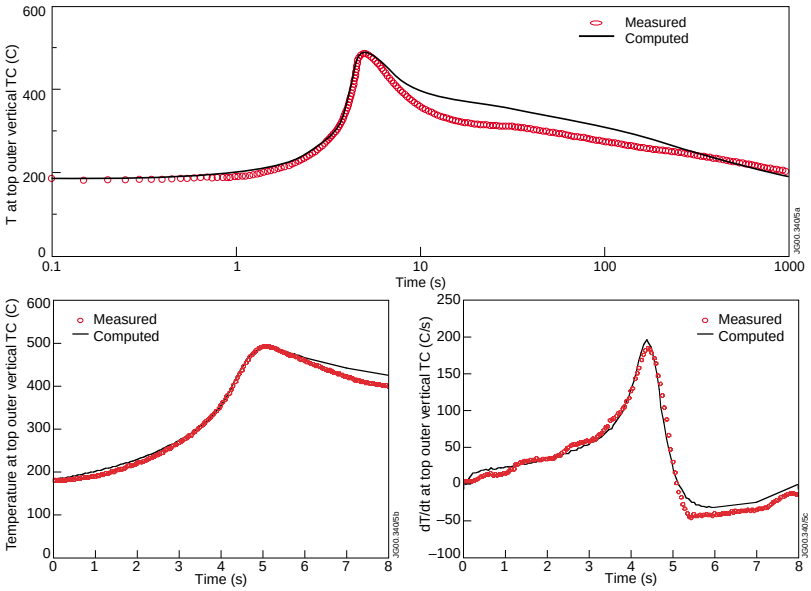

Figure 5: Temperature with (a) and without (b) the cooling phase and time derivative of the temperature (c) at the top thermocouple of the outer vertical target tile for pulse 50397 (16 MW, 16 mm/s, no additional D-puffing)

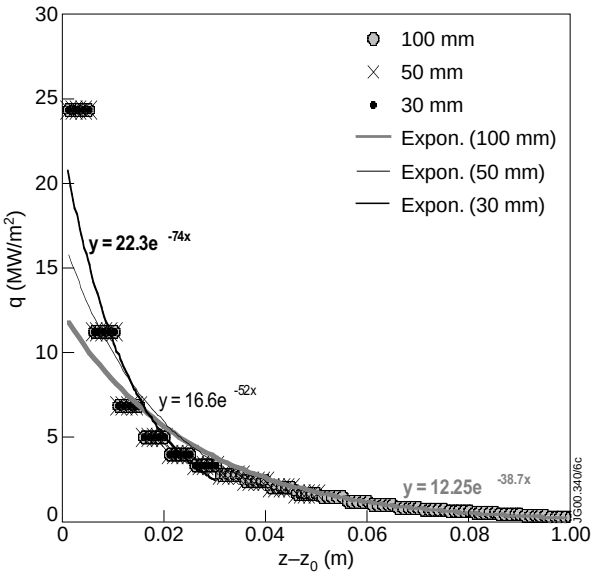

Figure 6: The power profile which matches the measured temperature in pulse 50397 fitted with a single exponential on 3 support lengths (z-z$_0$= 30 mm, 50 mm and 100 mm).

in the time derivative of the temperature, the initial position of the strike-point shift is fixed too. The total leg power, P_{leg}, is determined by the long-term temperature increase of the tile. We are then left with three variables: the ratio between the power going into the thin and wide exponentials ($C=P_W/P_T$), and the decay lengths of the wide (l_W) and the thin (l_T) exponentials. The magnitude and the width of the peak of the time derivative of the temperature strongly depend on l_T. The tail of the time derivative depends on P_W/P_T and weakly on the wide decay length, l_W.

Once the profile shape has been adjusted to fit the experimental data, it can be re-fitted to a single exponential. If the profile contains a double exponential structure, then the e-folding length of the re-fitted exponential may depend strongly on the specified range (Figure 6); otherwise, the e-folding lengths are independent of the range.

3. ACCURACY OF THE METHOD

3.1 Distance from the exposed surface

The thermocouples give an integral measure of the power deposited on the surface above them and then conducted to the thermocouple location. As the TC conduction time, ~0.6 s, is much

ELMs. In addition, the finite distance from the surface may underestimate the total conducted power in presence of a surface layer. The exposed surface is likely to be left at a higher temperature than it would, had the conduction been ideal, so a larger fraction of the power reaching the target can be lost to radiation instead of conducted into the bulk. As the conductivity in the poloidal direction is a factor of 4 smaller than in the toroidal and across directions, the spreading of the temperature profile from the surface to the thermocouple is limited. Therefore a characteristic length similar to the distance from the exposed surface (10 mm) can be resolved.

3.2 Hole behind the thermocouple

Another potential limitation of the thermocouples is the need to have a hole piercing from the back of the tile to the thermocouple itself. This removes some material, and therefore a heat sink and a conduction medium, leading to the formation of a hot spot on top of the thermocouple. A 3D model with coarser mesh has been developed to quantify the error due to this. Two cases have been modelled: a non-shifted plasma (50431 has the heating and puffing characteristics as 50397, so the same power deposition profile has been used, but the strike-point is kept just below the thermocouple) and a spatially uniform 20 MW/m^2 power load with a 2 s duration.

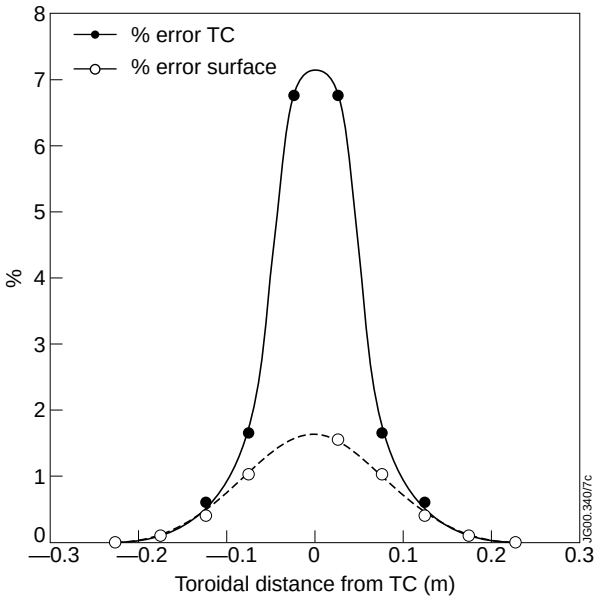

Figure 7: Temperature variation along the toroidal direction due to the thermocouple hole

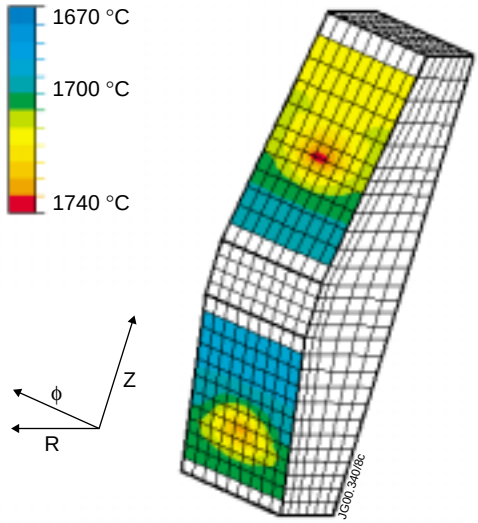

Figure 8: Hot spots on top of the thermocouple holes after 2 s of a spatially uniform 20 MW/m^2 power pulse.

The temperature has been collected along two sets of toroidal lines: one passing through the thermocouples and the other on the exposed surface above the thermocouple. For the unshifted plasma (Figure 7), the percentage increase of the temperature above the thermocouple is 1.5% and at the thermocouple 7% (this is larger as it is closer to the region where the heat sink is taken away by the hole). The percentage increase is slightly higher in the uniform constant load case (Figure 8).

3.3 Variations in the perpendicular field line angle

All the experiments analysed in this paper have been run with a very similar plasma configuration: low triangularity at 2.5 MA / 2.4 T. Only the divertor and the imbalance currents change as much as needed to move the plasma vertically and the poloidal beta increases slightly with the heating power. A typical fast shift experiment has been modelled with Proteus [8] in order to compute the perpendicular field line angles along the tile surface and their variation as the strike-point is shifted upwards.

The perpendicular field line angle, $q_{\perp}$, on the outer tile varies between 2.5^0 and 4^0 for the low strike-point configuration and between 3.5^0 and 5^0 for the high strike-point configuration. The toroidal fish-bone chamfer angle of these tiles is about 0.5^0, a, therefore the toroidal wetted fraction, defined by

$$TWF = \frac{\sin\theta_{\perp}}{\sin(\theta_{\perp} + \alpha)},$$

is always between 83% and 91% (Figure 9). This means that assuming profile shape remains constant as the strike-point moves leads to an error of ±4%. Both with PROTEUS and in EFIT the strike-point $\theta_{\perp}$ varies by less than a degree (3.5^0 to 4.5^0) along the shift. Consequently the TWF at the strike-point varies between 87.5% and 90% (the error at the strike-point, where the power density is higher, is <3%), while the ratio between power parallel to the field line and power projected to the tile surface, $q_{//}/q(z)$, varies between 14.3 and 12.7 (almost 12% error on the parallel power density). Additional inaccuracies are possible on the midplane decay length due to the flux expansion not being constant along the shift of the strike point. The flux expansion is ~4.5, it is slightly lower at the bottom (≥4) of the shift than at the top (≤5).

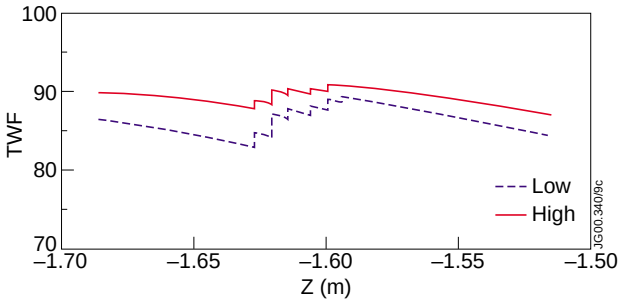

Figure 9: Toroidal wetted fraction as a function of the tile vertical co-ordinate computed for the configurations with the lowest and the highest strike-point positions.

4. VALIDATION

4.1 Power deposition profile shape

In 1999 a series of pulses was carried out in order to study the power deposition profile at JET [6]. All these pulses were ELMy H-modes (2.5 MA / 2.4 T with 12 MW neutral beam heating power) and had high clearance from the septum with the strike-point on the vertical target. The high clearance was needed in order to avoid affecting the plasma configuration when the strike-points were shifted up the vertical targets on a pulse by pulse basis. The power deposition profile was obtained from the pulse to pulse derivative of the deposited energy on the lower

vertical target tile with respect to the vertical position [6]. The slowly shifted discharges analysed in this paper are very similar to those in [6]: same plasma current and toroidal field; but no current in the outermost divertor coil, this may reduce the flux expansion. The shape of the power deposition profile obtained from the pulse by pulse strike-point shift matches the simplified profile used to fit the thermocouple measurements in the slowly shifted discharges with the same heating power, both at the outer (Figure 10) and at the inner (Figure 11) target.

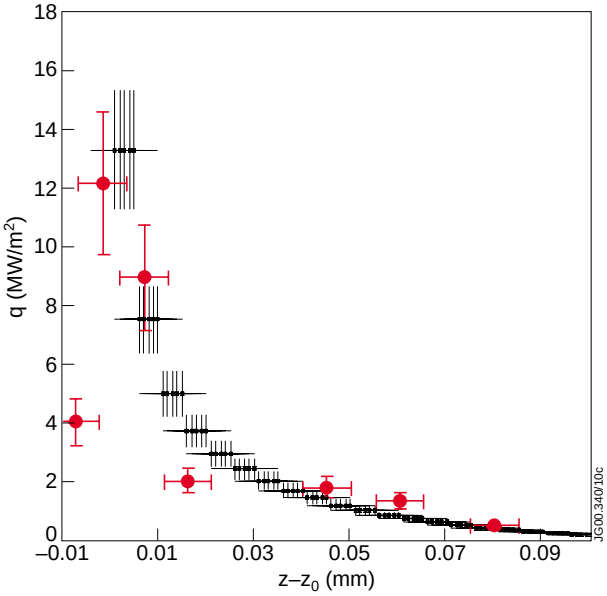

Figure 10: Power deposition profile at the outer target obtained from the pulse by pulse strike-point shift overlaid with the one best fitting the thermocouple data for pulse 50401 (12 MW, no D-puffing)

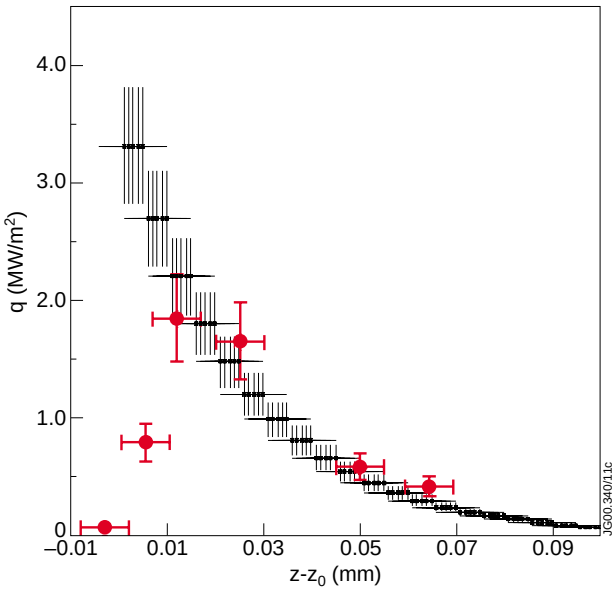

Figure 11: Power deposition profile at the inner target obtained from the pulse by pulse strike-point shift overlaid with the one best fitting the thermocouple data for pulse 50401 (12 MW, no D-puffing). The poor fit can be ascribed to the unsuitability the exponential profile prescribed in the simulations to fit the measured skewed gaussian profile.

4.2 Energy partition

The partition of energy between the outer and the inner target is very similar in both sets of discharges (Figure 12). The outer target collects more than 3 times the energy collected by the inner (Figure 13). Although the data covers both L-mode and ELMy H-mode confinement regimes, the power split between outer and inner target is roughly constant, i.e. not affected by ELMs. Since the ELMs are responsible for up to 30% of the energy arriving at the divertor targets [6], this implies that either the outer/inner asymmetry in power deposition remains unchanged during an ELM event or the inter-ELM power asymmetry compensates for the one during the ELMs.

The ELM frequency is ~10 Hz in these discharges. When the strike-points are moved at 16 mm/s an ELM hits on average every ~1.6 mm. This being less than a tenth of the vertical decay length, the ELM profile is averaged out in the power deposition profile.

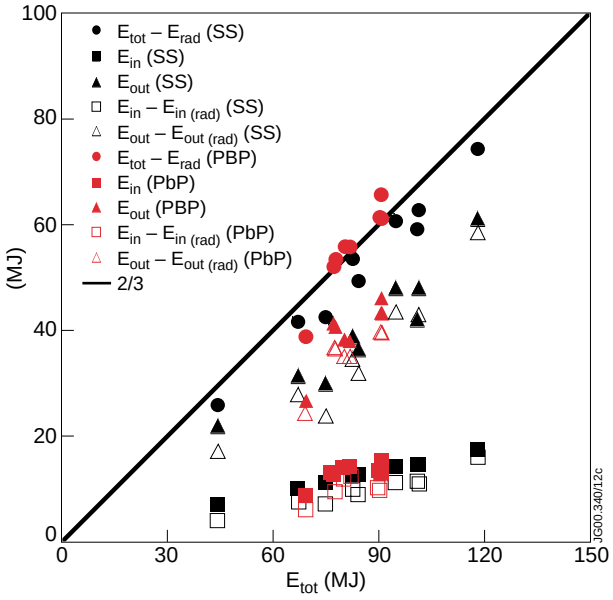

Figure 12: Energy partition between the inner and the outer targets, with and without radiation, for both the slowly shifted [SS] discharges and the pulse-by-pulse discharges [PbP]. E_{tot} is the total input energy (time integral of the heating power). E_{rad} is the total radiation (estimated using bolometry). E_{in} is the energy arriving at the inner target and E_{out} at the outer target (taken from the target thermocouples); for these the radiation is estimated from the unloaded horizontal tile.

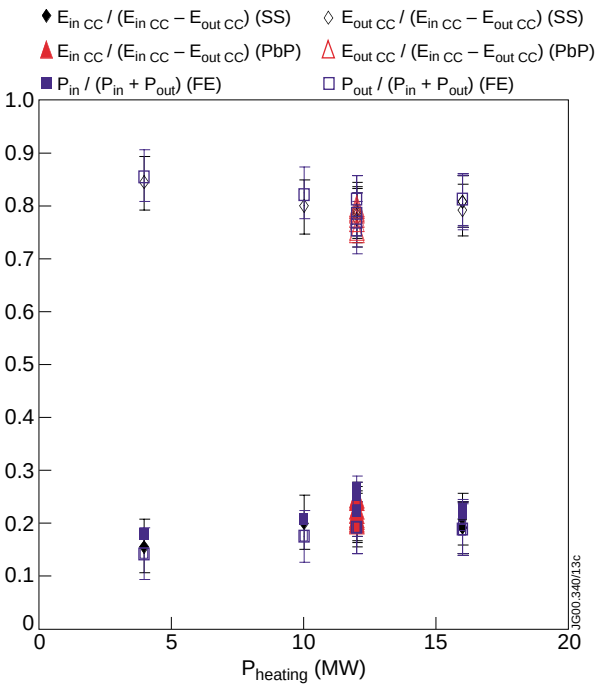

Figure 13: Fraction of convective and conductive energy (E##CC=E##-E##(rad)) received by the inner and outer targets in the slowly shifted [SS] discharges and in the pulse-by-pulse [PbP] discharges, compared with the fraction of power [FE] needed to fit the thermocouple measurements in the simulation of the slowly shifted discharges.

4.3 Strike-point velocity

The temperature change inside a semi-infinite slab due to a power glitch, q_0, at the surface lasting from t_1 to t_2 is [9]

$$T(x,t) - T_0 = \frac{q_0}{k}\left(\Theta(x,t-t_1) - \Theta(x,t-t_2)\right),$$

with

$$\Theta(x,t) = \sqrt{\frac{4\,\alpha\,t}{\pi}}\,exp\left(-\frac{x^2}{4\,\alpha\,t}\right) - x\left(1 - erf\left(\frac{x}{\sqrt{4\,\alpha\,t}}\right)\right),$$

where $\alpha = k/(\rho\, c_p)$, k being the thermal conductivity, ρ the density and c_p the specific heat. For an isotropic medium, the shift of the strike-point can be simplified as a variable distance of the point where the temperature is calculated from the heated surface. In the CFC case, the equivalent distance is $x = d(t) = \sqrt{x_0^2 + \left[\frac{\alpha_{pol}}{\alpha}\left(v_y t - \frac{H}{2}\right)\right]^2}$. Here x_0 is the distance of the thermocouple from the surface, v_y is the strike point velocity, H is the length of the path covered

by the strike point (assuming the thermocouple is in the middle) and α_{pol} is on the low conductivity direction. The temperature at the thermocouple can then be estimated for several strike-point velocities. Using the properties of the tile CFC, the maximum time derivative of the thermocouple temperature shows a peak for velocities in the range 6-40 mm/s (Figure 14). A similar analysis has been performed on a 2D FE model, for a limited number of velocities. Its results confirm that the best time response can be obtained with velocities in the range 10-40 mm/s (Figure 15).

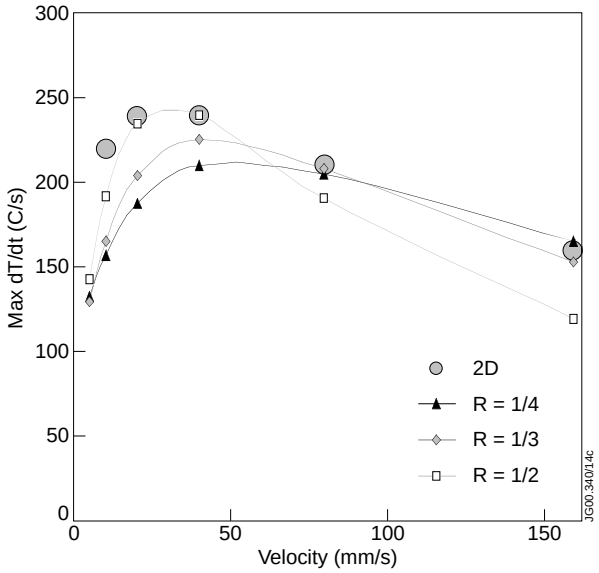

*Figure 14: 1D analytical estimate of the peak of the time derivative of the thermocouple's temperature as a function of the shift velocity for some shift velocity and a few ratio of poloidal to across conductivity (*R*), overlapped by the 2D FE results*

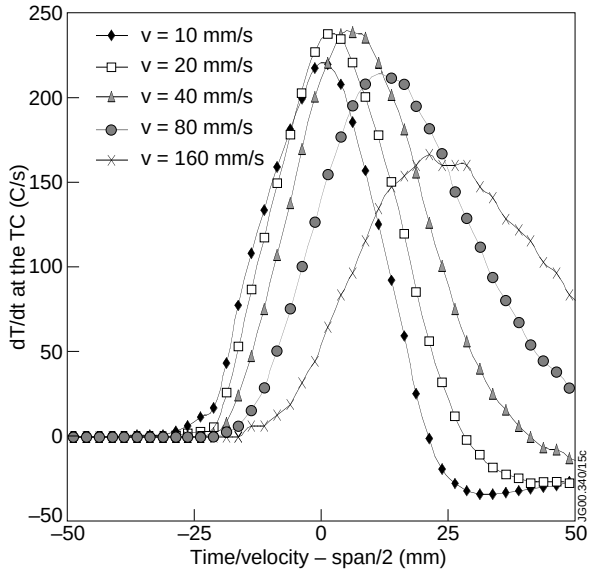

Figure 15: Time derivative of the thermocouple's temperature versus normalised time for 5 strike-point shift velocities (2D FE simulation)

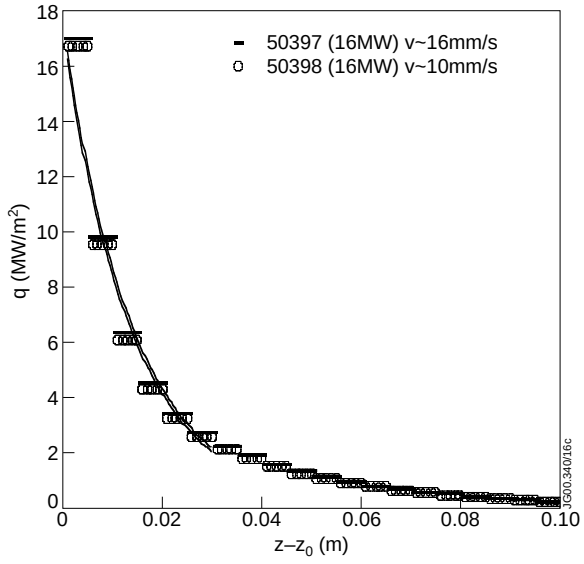

Figure 16: The power deposition profiles matching two of the 16 MW discharges: pulse 50397 (16 mm/s) and 50398 (10 mm/s); both discharges were without additional D-puffing.

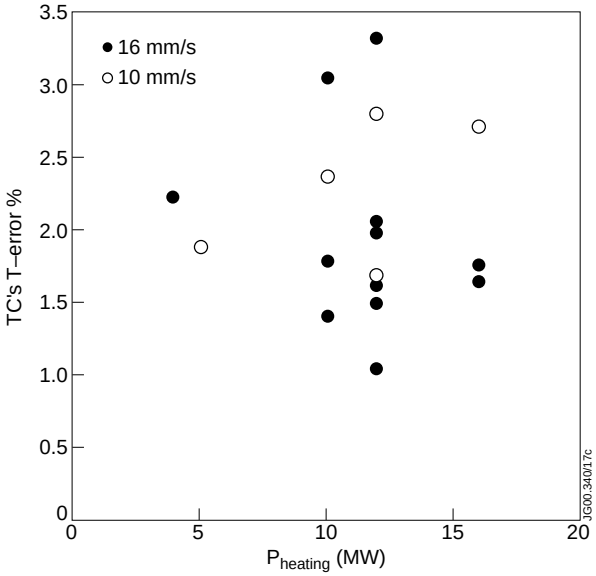

Figure 17: Relative error in temperature at the top outer vertical target thermocouple in the slow shift discharges

Most of the discharges have been run with a shift velocity of 16 mm/s, but some at 10 mm/s. Usually the best fit power deposition profile for pairs of discharges with different shift velocity and the same additional heating and D-puffing are very similar. This shows that the plasma configuration and the power deposition profile are not affected by this change in strike-point shift velocity. The power deposition profiles of two 16 MW discharges without additional D-puffing are plotted in Figure 16.

4.4 Fitting errors

For all the analysed discharges the thermocouple relative error in temperature (Figure17) has been estimated as

$$\frac{1}{T_{average}} \int_0^t \left| T_{measured} - T_{computed} \right| dt'$$

where t is the duration of the additional heating pulse.

Table 1

Absolute errors from scanning on the profile free parameters for pulse 50397; the absolute error in temperature is defined as $\frac{1}{t}\int_0^t \left| T_{measured} - T_{computed} \right| dt'$ *and in time derivative of the temperature as* $\frac{1}{t}\int_0^t \left| \dot{T}_{measured} - \dot{T}_{computed} \right| dt'$*, where the integration interval is either the additional heating pulse (average) or the across the half width of the time derivative peak.*

λ_T [m]	λ_W [m]	C	eT_{peak} [C]	$eT_{average}$ [C]	$e(dT/dt)_{peak}$ [C/s]	$e(dT/dt)_{average}$ [C/s]
0.004	**0.03**	**1.65**	**20.8**	**4.9**	**16.8**	**7.5**
0.001	0.03	1.65	32.0	18.9	22.6	14.8
0.01	0.03	1.65	34.9	14.7	18.5	10.6
0.004	0.03	**1**	19.8	8.5	17.8	11.2
0.004	0.03	**3**	24.0	12.9	18.7	8.8
0.004	**0.2**	1.65	26.8	8.6	17.4	10.1
0.004	**0.5**	1.65	16.5	14.7	18.6	13.1

On a single shot (50397), the three free parameters (l_T, l_W, C) have been varied and the effect of their variation on the error during the additional heating pulse and at the time the strike point is closest to the thermocouple has been computed (Table 1). Although the best-fit parameters have been tuned on the average errors for the temperature and its time derivative, they give the smallest error also on the peak values.

5. RESULTS AND DISCUSSION

The power decay length on the outer vertical target is plotted in Figure18 for the discharges without puffing. As the profile is a combination of exponentials, the decay width of the exponential fit depends on the length on which it is requested. In Figure18 the scalings on *z*-*z*0= 30 mm and 100 mm are plotted together with the integral power width [5], defined as

$$\lambda_q = \int_0^L q(z)\,dz \Big/ q(z=0)$$

Figure 18 shows that the L-mode contains only a single exponential, while the H-mode contains a double exponential feature: a wide exponential of the same width as the L-mode and a thin exponential which becomes progressively narrow as the heating power increases. The scaling with outer leg power, P_{outer}, of the decay width in the 30 mm fit and in the integral definition are very similar, both going as $P_{in}^{-(0.4\Pi 0.45)}$. This is consistent with the scaling of the peak power density with the outer leg power ($P_{outer}^{1.4\Pi 1.45}$) plotted in Figure 19, as $q\mu P_{leg}/l_q$. In Figure19 both the total peak power density, $q(z=0)$, and the wide exponential contribution to the peak power density, $q_W(z=0)$, are plotted; the latter has an off-set linear scaling with the leg power.

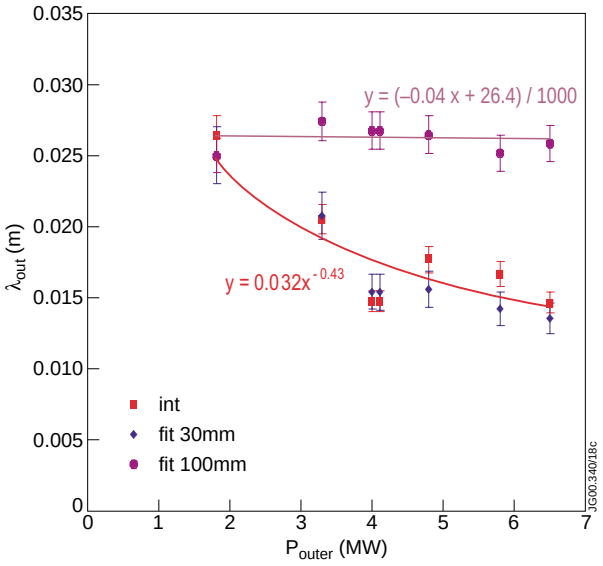

Figure 18: Outer vertical power decay length for discharges without D-puffing (the flux expansion at the outer vertical target is ~4.5: 27 mm correspond to ~6 mm-midplane)

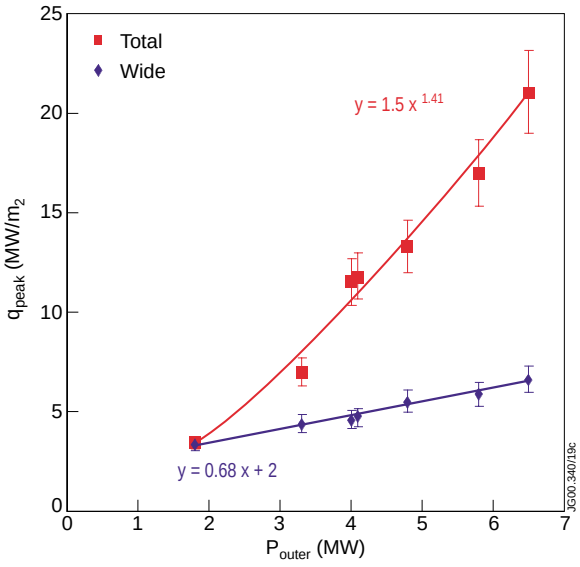

Figure 19: Peak of power density projected on the outer divertor for discharges without D-puffing (the power density parallel to the field lines is ~13.5 times the projected)

The fraction of the heating power reaching the outer divertor slightly decreases as leg power increases. The way the leg power is split between the wide and thin exponentials changes significantly with the leg power: the fraction going through the thin feature increases linearly with the leg power (Figure 20).

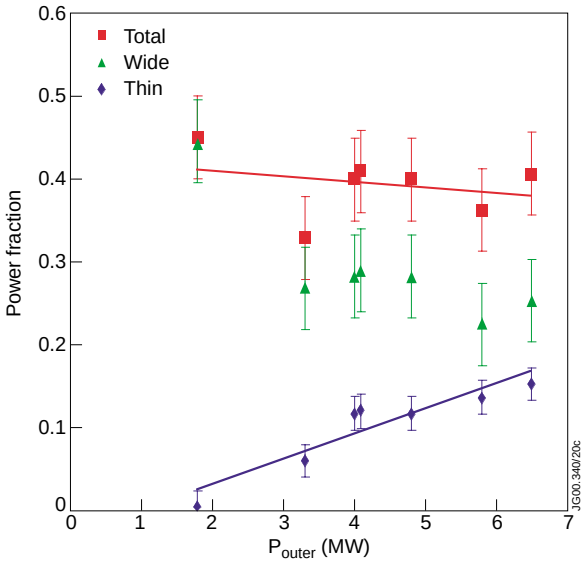

Figure 20: Fraction of heating power conducted to the outer divertor. Squares for the total, triangles for the wide and diamonds for the thin decay length contributions

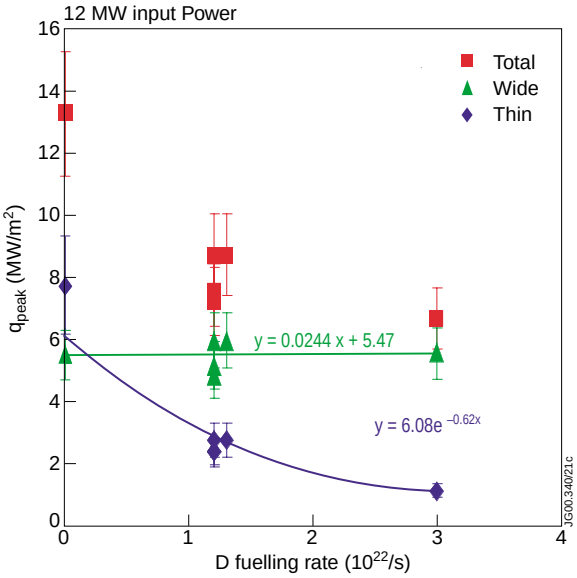

Figure 21: Power density peaks (squared for total, diamonds for thin and triangles for wide exponential) for D-puffed experiments with 12 MW heating power

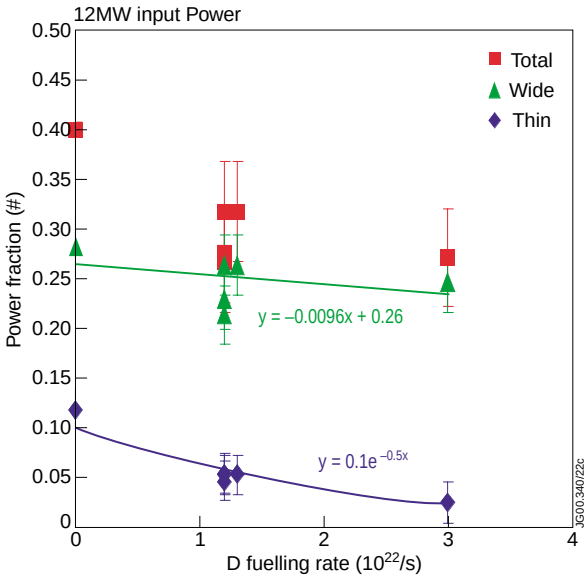

Figure 22: Fraction of heating power conducted to the outer divertor for different rates of D-puffing with 12 MW of heating power. Squares for the total, triangles for the wide and diamonds for the thin decay length contributions.

In the puffed experiments, with D-fuelling rate up to 3 10^{22} s^{-1}, the peak power density decays with increased puffing, while the wide exponential contribution remains roughly constant (Figure 21). Also the fraction of power convected/conducted long the leg to the divertor decreases (Figure 22). The contribution of the thin feature decreases more than the one of the wide base of the power deposition profile.

The accuracy of the inner divertor results is inferior to the outside: the conducted power is much smaller and the effect of the ELMs larger. The inner divertor fitting was done differently from the fitting at the outer divertor: a single decay length has been used and only the peak of the temperature time derivative has been matched (not the full response waveform as at the outer divertor). Within the rather broad error range, the power deposition decay length does not depend on the inner leg power (Figure 23) and the peak power density scales linearly with the leg power (Figure 24).

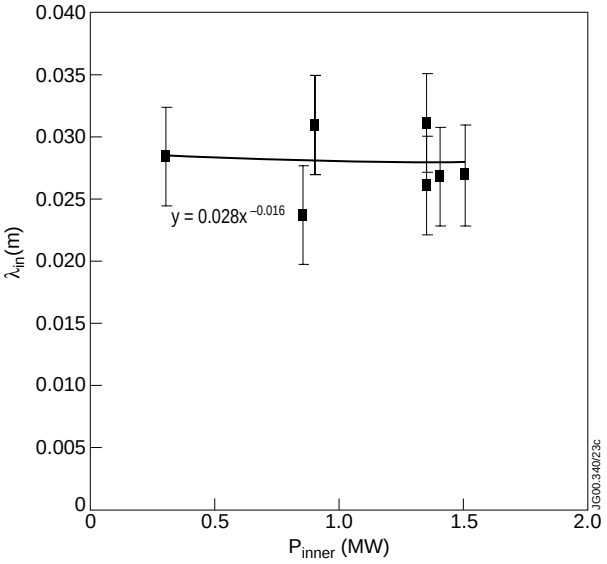

Figure 23: Inner vertical power deposition decay length

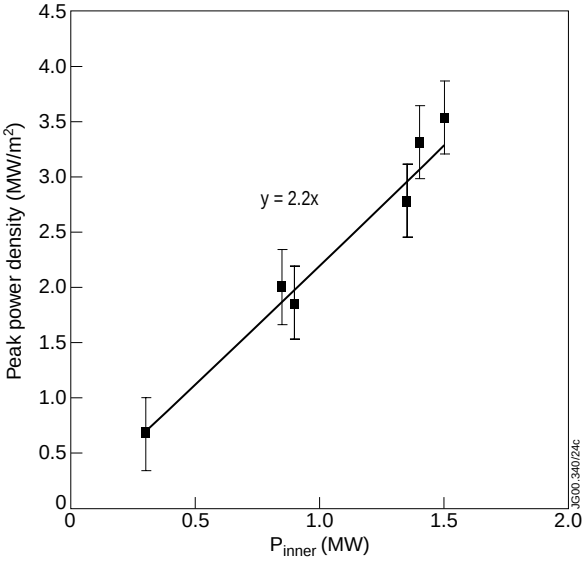

Figure 24: Inner peak power density (with and without D-puffing)

6. CONCLUSION

The power deposition profiles obtained shifting slowly the strike-points along the vertical targets have been proven consistent with those reconstructed using a pulse-by-pulse approach. This novel technique has the advantage of allowing the investigation of a wide range of heating and fuelling boundary conditions while making use of a limited number of discharges. However, this technique can only be applied to some plasma configurations: for the time being it can be exploited only by vertical target configurations, but when the MkIIGB septum and dome are removed shifts will be possible also on the horizontal target).

In addition the scenarios must be robust to strike-point displacement, this is not applicable to ITBs which have the location of the outer strike-point constrained by the pumping needs. In the limited set of plasma configurations where thermocouples can be employed to investigate the power deposition profile, they are only complementary to infra-red cameras and Langmuir probes (e.g. the time resolution at the thermocouples is too poor for ELM detection and analysis).

The accuracy of the results is better at the outer than at the inner target, because the power collected at the outer is much larger (and hence the quality of the measurements). For the very same reason, collecting information on the outer target is more important for the design of future devices.

The thermocouple data has been used to estimate the power deposition profile of a set of 2.5 MA 2.4 T plasmas. In L-mode plasmas the profile has a single scrape-off decay length, in H-mode plasmas a thin feature is evident at the outer target, which disappears when the edge density is increased by puffing. These discharges will be discussed further elsewhere.

ACKNOWLEDGEMENTS

The authors wish to thank the members of the Task Force E and in particular T. Eich, A. Hermann, A. Kallenbach and M. Laux.

This work was performed partly in the framework of the JET Joint Undertaking and partly under the European Fusion Development Agreement (EFDA). The latter part was funded under the JET Operating Contract by EFDA.

W. Fundameski would like to acknowledge the support of the Canadian Natural Science and Engineering Research Council.

REFERENCES

[1] R.R. Parker et al., *ITER in-vessel system design and performance*, Nuclear Fusion **40** (2000) 473-484

[2] R.J. Thome, *Engineering Overview of the Fusion Ignition Research Experiment (FIRE),* Proc. 18th SOFE, Albuquerque, October 1999

[2] J. Pamela, *JET under EFDA*, Proc. 21st SOFT, Madrid, September 1999

[4] K. McCormick et al., *ITER Edge Database Investigations of the SOL Width*, Journal of Nuclear Materials 266-269 (1999) 99-108

[5] A. Loarte et al., *Multi-machine scaling of the divertor peak heat flux and width for L-mode and H-mode discharges*, Journal of Nuclear Materials 266-269 (1999) 587-592

[6] G.F. Matthews et al.zs, *Divertor Energy Distribution in JET H-modes*, Proc. of the 14th PSI, 2000 (to be published in Journal of Nuclear Materials)

[7] H. Altmann et al., *The Use of Carbon Fibre Composites in Divertor Target Plate Tiles and Structures,* Proc. of the 16th SOFE, Champaign, October 1995

[8] R. Albanese et al., *Numerical Studies of the Next European Torus via the PROTEUS Code*, Proc. of the 12th Conf. On the Numerical Simulation of Plasmas, San Francisco, 1987

[9] J.P. Holman, *Heat Transfer,* 5th Ed., McGraw-Hill, New York, 1981 (p. 116)